Title

Reprint of: Inversion of dynamical Bragg intensities to complex structure factors by iterated projections. For Ultramic. 2020. ("Pico" Festschrift, May 2021)



Authors

Spence, John CH

Donatelli, Jeffrey J

Publication Date

2021-12-01

DOI

10.1016/j.ultramic.2021.113409

Peer reviewed

# Inversion of dynamical Bragg intensities to complex structure factors by iterated projections.

For Ultramic. 2020. ("Pico" Festschrift, May 2021)

John C.H. Spence and Jeffrey J. Donatelli[1,2]

Department of Physics, Arizona State University, Tempe, Arizona, 85287-1504 USA.

[1]Department of Applied Mathematics, Lawrence Berkeley Laboratory, Berkeley, CA 94720 USA.

[2]Center for Advanced Mathematics for Energy Research Applications, Lawrence Berkeley National Laboratory, Berkeley, CA 94720 USA

Abstract.

A method for recovering complex structure factors from many simultaneously excited Bragg beam intensities is described. The method is applied to simulated transmission electron diffraction data over a wide range of crystal thickness and beam energies. The method is based on iterated projections between structure and scattering matrices, which are related by a unitary transformation, which we invert. The algorithm removes multiple-scattering perturbations from diffraction data and might be extended to other fields, including X-ray and neutron diffraction and cryo-electron microscopy. Because coherent multiple scattering involves interference between Bragg beams, the method also solves the phase problem. Unlike dynamical inversion from electron microscope images or ptychography data, the method, which starts with Bragg beam intensities, provides complex structure factors unaffected by focusing errors or resolution limitations imposed by lenses. We provide inversions from simulated data with 441 simultaneously excited Bragg beams over a range of thickness and beam energy. We discuss the retrieval of chirality information from enantiomorphs, the efficient incorporation of symmetry information using the irreducible representation of the group of structure matrices, and the effect of HOLZ lines to provide three-dimensional information.

## 1. Introduction.

The lack of reproducibility of transmission electron diffraction (TED) data has always been considered a weakness of the method by advocates of X-ray crystallography, limiting its status and popularity among crystallographers, despite impressive recent advances in protein electron nanocrystallography [1]. Where crystals less than a few tens of nanometers thick can be prepared, there has also been recent success solving inorganic structures by TED (2). X-ray Bragg beam intensities measured on successive occasions from different specimens of the same crystal, differing in size, give closely similar intensity ratios, whereas for electron diffraction small changes in crystal thickness causes large changes in Bragg beam intensities, as a result of multiple scattering. Kinematic electron scattering for light-element inorganics is limited to a few hundred angstroms in thickness or much less for heavier atoms. This sensitivity of TED to thickness has been turned to an advantage for the imaging of stacking faults and dislocation cores [3], and for imaging surface steps, crystal growth and oxidation, all using forbidden reflections [4]. The much stronger interaction of electrons has also made multiple scattering useful for space-group determination of nanocrystals by convergent-beam electron diffraction [5], and for distinguishing enantiomorphs (such as the hand of quartz [6]), an especially important problem in the drug industry, where this chiral determination problem has recently been addressed for pharmacological compounds by TED [7].

We have recently described [8] a method for recovering the same complex structure factors of a crystalline TEM sample from Bragg spot intensities over a very wide range of thickness and electron beam energy. This solution to the inversion problem of dynamical diffraction removes multiple scattering artifacts from diffraction data. It extends the range to small and much larger thickness of our earlier method, based on iterated projections [9, 10]. Because multiple scattering involves interference between coherent Bragg beams, this also solves the phase problem. Unlike alternative successful approaches based on STEM images [11] our method inputs far-field diffracted intensities, making our retrieved structure factor phases independent of the resolution imposed by the instrument, and of instrumental phases, due to focusing and aberrations. This provides a robust method which is also independent of sample movement (for a parallel-sided crystalline slab). In this paper we briefly review the method and discuss its experimental implementation, and the possibilities for using symmetry reduction to reduce the amount of data needed.

The inversion problem of multiple scattering has a long history (see [8, 5] for references). A general solution to this problem would have applications in many fields, from optical ptychography, to neutron diffraction and the weak low-order reflections, most sensitive to chemical bonding, in inorganic X-ray crystallography, where primary extinction (multiple scattering) is strongest. Its extension to non-periodic samples would increase the size of the macromolecules which can be faithfully imaged in cryo-EM, and so facilitate whole-cell imaging.

## 2. Formulation of problem

Our approach is based on the scattering matrix defined by Niehrs, Sturkey [12] Fujimoto [13] and studied in detail for the purposes of inversion twenty years ago by Allen et al [14] and

Spence [15]. (For a review of dynamical theory, see [16]). Here, our earlier algorithm [9] is extended to small thickness (where the Bragg intensities do not carry phase information) by using the "charge-flipping" algorithm [16], and to very large thickness by identifying and eliminating a previous source of instability in the forward calculation, and several other important developments. The charge-flipping algorithm, developed for phasing X-ray diffraction data, is akin to solvent-flattening methods, which drives the density to zero between atoms in crystals, since these consist mostly of empty space. It has been applied to solving inorganic nanocrystals by electron diffraction (where the potential, rather than the charge density is driven to zero) using the kinematic convergent beam (KCBED) method in recent work [17].

Sturkey's scattering matrix **S** gives the complex Bragg beam amplitudes $\phi$ diffracted by a thin slab of crystal of thickness t traversed by a high-energy collimated electron beam as entries in a column vector $\phi$, where $\phi = \mathbf{S}\,\phi_o$. Here for an incident beam $\phi_o$ travelling along the symmetric zone-axis direction, $\phi_o$ contains zeros expect for unity in the central position, and

$$\mathbf{S} = \exp(2\pi i \mathbf{A} t) \qquad 1$$

In this case, $\phi_o$ then picks out the central column of **S** (of order N) as the observable diffraction pattern. Moving the unity value in $\phi_o$ picks out other columns of **A** which describe diffraction from tilted orientations ([18]) with new incident beam directions differing by Bragg conditions, all of which must be recorded experimentally to fill out **S**. The structure matrix **A** of order N contains entries $\sigma V_g/(2\pi) = 1/(2\xi_g) = U_g/(2K)$ in off-diagonal positions, where the wanted structure factors $V_g$ (in volts) or $U_g$ (potential energy terms in **A**) are the Fourier coefficients of the scattering potential $V(\mathbf{r})$) . ($\xi_g$ is an extinction distance, $K \sim 1/\lambda'$ a corrected beam wavevector and $\sigma = 2\pi m |e| \lambda / h^2$ with m the relativistic electron mass. The diagonal of **A** contains known excitation errors $S_g = (-2\mathbf{K}_t \cdot \mathbf{g} - \mathbf{g}^2)/2K$. Here $\mathbf{K}_t = 0$ if the symmetric zone axis pattern is the central column (for lattice vectors $\mathbf{g} = \mathbf{g}$ (h,k,l)). These excitation errors define the diffraction conditions and kinetic energy (beam wavelength $\lambda$ and direction). For example, for N= 3 we have

$$\mathbf{A} = (1/2K) \begin{bmatrix} 2KS_g & U_g & U_{2g} \\ U_{-g} & 0 & U_g \\ U_{-2g} & U_{-g} & 2KS_{-g} \end{bmatrix} \qquad 2$$

Backscattering and polarization (important for the X-ray problem) are neglected in this scalar theory. The inversion problem consists in finding **A**, given the magnitude of the entries in **S** (Bragg beam intensities) and the diagonal of **A** (excitation errors). In the absence of absorption, equation 1 is a unitary transformation, which we aim to invert. If t is re-interpreted as time, then equation 1 gives the time-evolution operator in time-dependent quantum mechanics. Our algorithm includes a mean absorption coefficient on the diagonal, requiring repeated re-normalisation of **S**.

If imaging or ptychography are used to provide data [11,19], so that the *complex* entries in **S** are known, inversion is relatively straightforward using the logarithm of **S**. Then the known diagonal of **A** and its symmetries (including symmetry across the anti-diagonal) can be used to resolve the problem of branch cuts in the multi-valued complex logarithm function [14]. This also allows forward and reverse iterative computation [9] for the methods of non-convex optimization based on iterated projections [8] from measured intensities. It is remarkable that the thickness of the sample need not to be known. The principle of logarithmic inversion can be simply understood as follows. The eigenvalues $\lambda$ of **S** and $\gamma$ of **A** are related by

$$\lambda_i = \exp(2\pi i \gamma_i t). \qquad 3.$$

so that

$$\ln \lambda^i = i(\theta^i + 2n^i\pi) = 2\pi i \gamma^i t \qquad 4$$

With just two beams (to show the principle of the method) we have

$$2\pi i\mathbf{A}t = \ln \mathbf{S} = \mathbf{C}\begin{bmatrix} \ln\lambda^i & 0 \\ 0 & \ln\lambda^i \end{bmatrix}\mathbf{C}^{-1}$$

$$= 2\pi t\begin{bmatrix} S_g & U_g/2K \\ U_g/2K & 0 \end{bmatrix} = \mathrm{C}\begin{bmatrix} \theta^{(1)} + 2\pi n^{(1)} & 0 \\ 0 & \theta^{(2)} + 2\pi n^{(2)} \end{bmatrix} C^{-1} \qquad 5$$

This gives a set of linear equations between the diagonals on either side in equation 5, which may be solved for the branch indices $n^i$, assuming the excitation errors $S_g$ and complex **S** are known (e.g. from imaging experiments), and hence its eigenvalues $\lambda$ and $\theta^i$ in the range $-\pi/2$ to $\pi/2$. In general there are $(N^2-1)/2$ real unknown parameters in hermitian **A**, which also has anti-diagonal symmetry. This symmetry may be further increased by crystal symmetries. One requires as many linear equations as unknown values of $n^{(i)}$.

Each column of **S** contains the complex amplitudes of a complete two-dimensional diffraction pattern, with the axial zone axis pattern as the central column, and tilted patterns in the other columns. It follows that inversion from a single diffraction pattern is not possible. The beam tilts needed to fill the other columns require a reciprocal lattice vector to be added to $\mathbf{K}_t$ for each successive column, corresponding to the second-order Bragg condition for the first tilt, as explained in detail in [15] (equation 14). The first-order Bragg condition is satisfied by $\mathbf{K}_t = -\mathbf{g}/2$ [16]. These tilted diffraction patterns, in columns in **S** must be measured experimentally using different incident beam directions. We discuss below the reduction in the amount of data needed if crystal symmetries are present.

The relationship between the three Miller indices defining reciprocal lattice vectors **g** and the two-dimensional indices of matrices **A** and **S** can be understood from the small thickness (single scattering) limit, which allows a first-order expansion of equation 1, where the Miller indices of **S** are given by the corresponding entries in **A**. The crystallographic indices of the central column of **S** and **A** (provided by the zone-axis indexed experimental pattern) equal those of the diagonal, which fix the indices of all other entries, as in equation 2. This is exactly analogous to one-electron band structure theory for crystal electrons, with **A** the Hamiltonian matrix. As in that

case, diagonal terms describe kinetic energy, while off-diagonal terms describe potential energy, Bloch waves are periodic in **k**-space, as are their eigen-energies, according to a three-dimensional Brillouin zone construction. Our TED Brillouin zone for $\mathbf{K}_t$ is two-dimensional.

Assume that the excitation errors on the diagonal of **A** are arranged symmetrically, with zero at the center of the matrix. If the inversion process commenced with the filling of **S** (not **A**), this would require assignment of Miller indices to **S**. The Miller indices for the entries in columns of **S** are equal to the corresponding entries in **A** for a small-thickness expansion of the exponential. The indexing sequence along the diagonal fixes all indices throughout the matrix, and is the same as that down the central column.

Each column of **S** contains the complex Bragg amplitudes for a two-dimensional diffraction pattern for some incident beam direction. This direction is defined by the one excitation error in the corresponding column of **A**, which in turn defines a value of $\mathbf{K}_t$ which can therefore be used to label each column in **S**. For symmetrically arranged excitation errors on the diagonal of **A**, the column observed experimentally in **S** is always the central column, even for a tilted beam calculation with different excitation errors on the diagonal. As shown elsewhere [15], because of the eigenvector periodicity relations given below, tilting the beam so that the scattering vector $2\mathbf{K}_t$ satisfies the Bragg condition brings the column labelled $\mathbf{K}_t$ in **S** into the central observable condition. In the systematics case (where a line of Bragg reflections is excited) it will be seen that the scattering matrices evaluated with excitation errors for $\mathbf{K}_t=n\mathbf{g}(100)$ (reflection $2\mathbf{K}_t$ at Bragg condition) is identical to that for $\mathbf{K}_t=0$ with different (symmetric) excitation errors on the diagonal of **A**, except for a shift of all entries by n places down and across in **S**. In both cases only the central column is observable. The equality of these columns in **S** when computed using different excitation errors can be understood in several ways. The form of the excitation errors (a function of $(\mathbf{K}_t-\mathbf{g})$ ) under tilting is such that a tilt causes them all to move along the diagonal, apart from an unimportant constant term (phase shift). This permutates the rows and columns of **S**.

A succession of tilted patterns therefore provides all the magnitudes needed to fill **S**. In the systematics orientation, adding a reciprocal lattice vector to $\mathbf{K}_t$ (initially zero in the symmetric orientation) excites every second Bragg reflection. Because of the periodicity relations, these orientations excite identical Bloch waves inside the crystal, which nevertheless generate different diffracted intensities as a result of matching this total wavefield to the slab boundary conditions. The periodicity relationships for eigenvectors and eigenvalues follow from the fact that the Bloch waves (but not the total wavefunction matched to boundary conditions) are periodic in reciprocal space (but not in real space), with the period of a two-dimensional Wigner-Seitz cell for $\mathbf{K}_t$. Bloch's theorem, (from Floquet) allows Bloch-wave solutions of the wave equation inside the crystal

$$b^{(j)}\left(\boldsymbol{K}_t^{(j)},\boldsymbol{r}\right)=\sum_g C_g^{(j)}\left(\boldsymbol{K}_t^{(j)}\right)\exp(2\,\pi\,i\,\left(\boldsymbol{K}_t^{(j)}+\boldsymbol{g}\right)\cdot\boldsymbol{r}) \qquad 6$$

After tilting, a reciprocal lattice vector **h** is added to $\mathbf{K}_t$, and this becomes

$$b^{(j)}\left(\boldsymbol{K}_t^{(j)}-\boldsymbol{h},\boldsymbol{r}\right)=\sum_l C_l^{(j)}\left(\boldsymbol{K}_t^{(j)}-\boldsymbol{h}\right)\exp(2\pi i\,\left(\boldsymbol{K}_t^{(j)}-\boldsymbol{h}\,+\boldsymbol{l}\right)\cdot\boldsymbol{r}) \qquad 7$$

For these to be equal for all $\mathbf{K}_t$, the coefficients multiplying the exponential must be equal, so that with $\mathbf{l} = \mathbf{g} + \mathbf{h}$, we must have [20]

$$C_g^{(j)}\left(\boldsymbol{K}_t^{(j)}\right) = C_{\boldsymbol{g}+\boldsymbol{h}}^{(j)}\left(\boldsymbol{K}_t^{(j)} - \boldsymbol{h}\right) \qquad 8$$

In addition, it can be shown that [21]

$$\gamma^{(j)}(\boldsymbol{K}_t - \boldsymbol{h}) = \gamma^{(j)}(\boldsymbol{K}_t) + S_{\boldsymbol{g}} \qquad 9$$

reflecting the well-known periodicity of the dispersion surfaces in many-beam dynamical theory.

### 3. The N-Phaser algorithm – simulation results.

Our method [8] iterates between complex **S** and **A.** Computational trials suggest that three constraints are then sufficient to define a "unique" solution, in the sense that multiple solutions are related by an origin shift in the recovered potential. This shift appears as a similarity transform on **S**, leaving eigenvalues unchanged. The search is non-convex. The three constraints are the symmetry constraints on **A**, its known diagonal, and the known magnitudes of the elements of **S**. The algorithm starts with a random 2D potential V(**r**), then iterates between **S** and **A** while repeatedly imposing these constraints on each. For each current estimate of **S**, phases are retained and magnitudes replaced with experimental values. Elements of **A** related by intrinsic and crystal symmetries are replaced by their symmetry-averaged values. An earlier version used an optimizer to iterate between the set of all **A** with correct symmetry and diagonal, and that of **S** with correct magnitudes [9]. This failed at small thickness (as expected, since kinematic intensities are not sensitive to structure factor phases), converged at moderate thickness (where multiple coherent scattering provides phasing) and failed at large thickness for reasons not understood at the time. This failure has now been understood to be due to the extreme sensitivity of $\lambda$ in forward calculations to small changes in $\gamma$ at large $t >> 1/\gamma$, leading to numerical instability. Equation 3 then cannot be used to reliably obtain $\lambda$ from $\gamma$. We now avoid this by using an optimizer to obtain $\lambda$ from the known magnitudes and eigenvectors of the current estimate of **S**, as shown in the flow chart of the algorithm given in figure 1. Thickness is not needed but may be refined in the flipping section. At moderate and small thickness, a modified algorithm is used which includes the charge-flipping algorithm, and uses logarithmic inversion discussed above with the known diagonal of **A** to determine the branch indices for the multivalued complex logarithm function. An optimizer is then not used. A number of other subtleties arise, such as the manner in which **S** is repeatedly made unitary, which are discussed in [8] and its Supplementary Information.

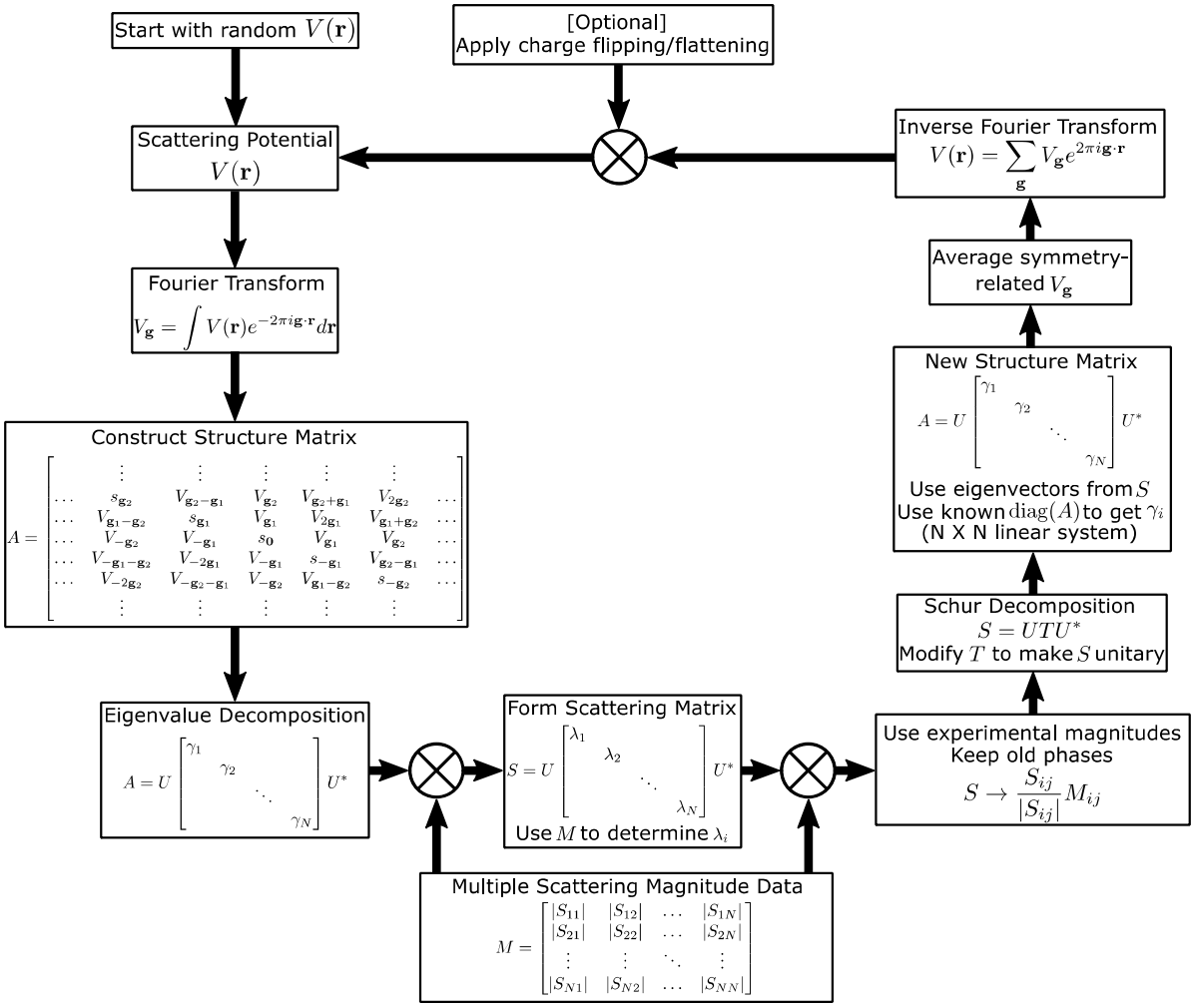


**Figure 1.** Flow chart of the version of the algorithm which determines the eigenvalues of **S** from the magnitudes of entries in **S** and its eigenvectors to avoid numerical instabilities at large thickness in the forward calculation. A second algorithm for moderate and small thickness uses logarithmic inversion. More detailed flow charts of both algorithms are given in [8]. To simplify notation, here we have included the factors of $\sigma/2\pi$ in the definition of Vg above. In computations, the entries in **A** should be those of equation 2.

Numerical trials have succeeded in recovering the potential for both GaAs and Spinel from simulated data over a range of beam energies from 100 kV to 1 MeV and thicknesses from 10nm to 1000 nm. Figure 2 shows reconstruction from the single-parameter Spinel crystal structure (with 71 atoms in the cubic cell) along the high-symmetry [100] direction using 441 beams. Because of this symmetry (as discussed below), it was found possible to obtain good reconstructions without requiring the large tilts needed to fill all the outer column of S, reducing the maximum tilt angle from 57 to 19 mrad. In these simulations, it was found that many entries in **S** were not needed, and could be left floating, greatly reducing the amount of data needed. For example, for Spinel, with N = 441 (and correlation coefficient 0.96), we were able to obtain a

reconstruction using only N = 221 with correlation coefficient 0.93. This symmetry in the diffraction patterns reduces correspondingly the number of linear equations in 3 which also express crystal symmetry. The same differences between Miller indices on the diagonal of **A** (which fix the position of off-diagonal entries) occur more than once, for example.

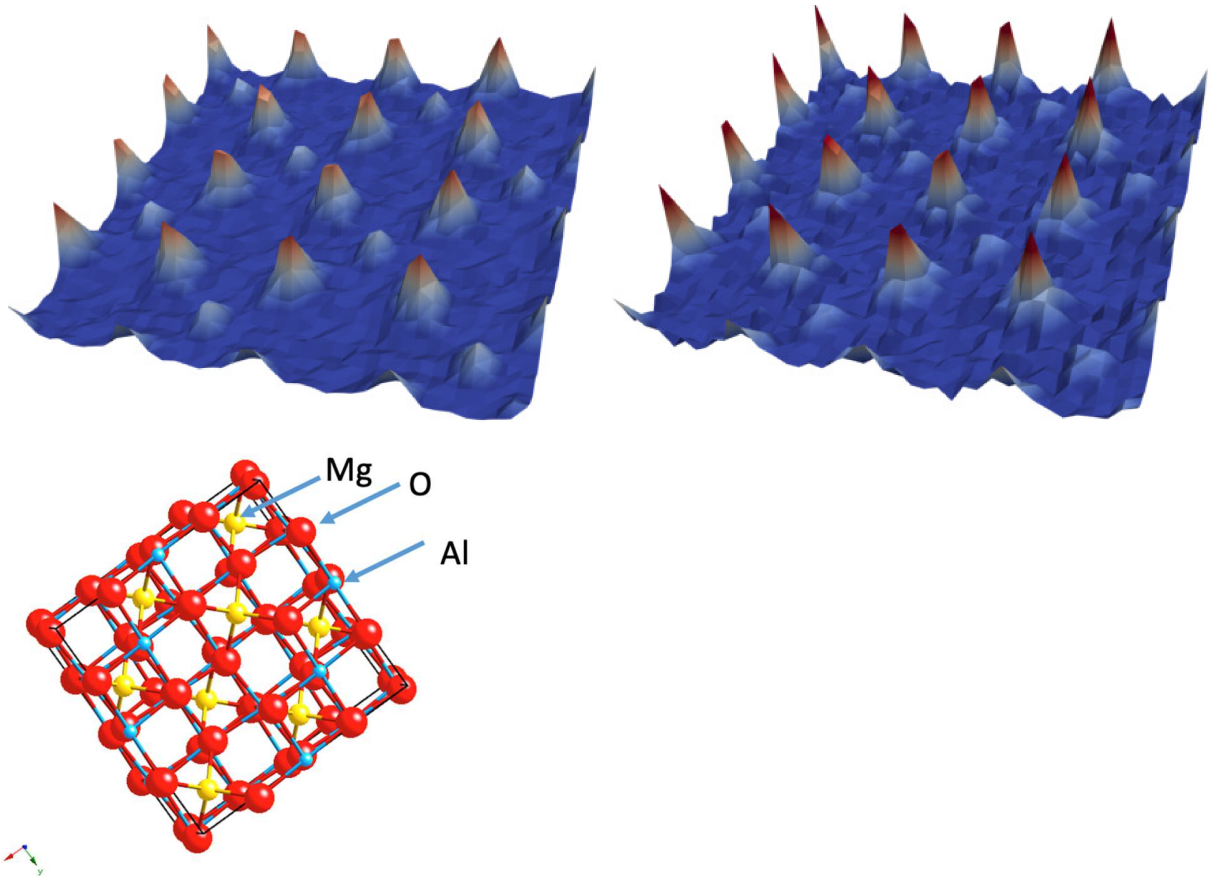


**Figure 2.** Recovery of Spinel crystal potential projected along [100] from 441 beam dynamical TED simulated diffraction pattern (LHS) compared with recovery using only 221 columns of the S matrix, greatly reducing the range of tilted diffraction patterns needed. Beam energy 300 kV, thickness 100nm. No flipping was used. Eigenvalues of S obtained from its magnitudes and eigenvectors. 200 iterations, about ten minutes on a laptop. Below, the spinel structure $MgAl_2O_4$.

Table 1 summarizes reconstructions from the acentric GaAs structure under many conditions, with thickness ranging from 10nm to 1000 nm (one micron), and beam energy from 100 kV to 1 MeV. Cases where $\lambda$ is obtained from A by logarithmic inversion or (at the largest thickness where this is not possible) from the magnitudes of **S** are shown, together with and without use of the flipping algorithm. Because the random starts results in different origins and complex structure factors for the reconstructions, we show the Pearson correlation coefficient between the original ground truth potential V(r) used to simulate the diffraction data and the recovered potential. Thickness estimates are also shown compared to actual thickness when $\lambda$ is computed logarithmically from A. In summary, only at 1 MeV for a thicknesses of 100nm and one micron

is it not possible to obtain a correlation coefficient above 0.9. Here the algorithm starts to fail at high beam energy as all the excitation errors become negligible due to the very flat Ewald sphere, and the system of linear equations relating branch cuts to the diagonal of **A** becomes homogeneous, so that these cannot be determined.

**Pearson Correlation Coefficients**

| | 10 nm | 100 nm | 1000 nm |
|---|---|---|---|
| 100 kV | 0.975 | 0.901 | 0.823 |
| 300 kV | 0.971 | 0.889 | 0.8 |
| 1000 kV | 0.971 | 0.837 | 0.574 |

Computes lambda from A
Thickness fixed
Flipping

| | 10 nm | 100 nm | 1000 nm |
|---|---|---|---|
| 100 kV | 0.463 | 0.732 | 0.559 |
| 300 kV | 0.451 | 0.4 | 0.582 |
| 1000 kV | 0.997 | 0.64 | 0.434 |

Computes lambda from A
Thickness fixed
No flipping

| | 10 nm | 100 nm | 1000 nm |
|---|---|---|---|
| 100 kV | 0.976 | 0.896 | 0.84 |
| 300 kV | 0.974 | 0.858 | 0.84 |
| 1000 kV | 0.971 | 0.812 | 0.697 |

Computes lambda from A
Computes thickness
Flipping

| | 10 nm | 100 nm | 1000 nm |
|---|---|---|---|
| 100 kV | 0.956 | 0.947 | 0.956 |
| 300 kV | 0.9 | 0.973 | 0.958 |
| 1000 kV | 0.815 | 0.695 | 0.67 |

Computes lambda from S magnitudes
Flipping

| | 10 nm | 100 nm | 1000 nm |
|---|---|---|---|
| 100 kV | 0.456 | 0.971 | 0.93 |
| 300 kV | 0.289 | 0.968 | 0.961 |
| 1000 kV | 0.968 | 0.736 | 0.774 |

Computes lambda from S magnitudes
No Flipping

**Computed Thickness**

| | 10 nm | 100 nm | 1000 nm |
|---|---|---|---|
| 100 kV | 10.2 | 30.2 | 1180 |
| 300 kV | 10.3 | 100.6 | 1196.8 |
| 1000 kV | 11.4 | 99.7 | 200 |

Computes lambda from A
Computes thickness
Flipping

**Table 1**. Correlation coefficients between ground truth and recovered potential for GaAs [110] zone axis transmission electron diffraction patterns using different methods for various beam energies and sample thicknesses.

## 4. Considerations for experimental implementation.

Long experience has shown that dynamical simulations match closely to elastically filtered convergent-beam electron diffraction patterns [5], giving confidence in this method when applied to experimental data if the **S** matrix can be accurately filled. Experimental tests using known inorganic structures are under way, using data collected on the ASU Titan 300 TEM/STEM fitted with Gatan spectrometer and CMOS detector, for the large dynamic range required.

This raises the question of the optimum data collection strategy for filling the matrix **S** from a series of tilted many-beam diffraction patterns, which frequently show high symmetry. For the Si [110] data we are collecting, the zone axis pattern contains two orthogonal mirror planes, so that it is only necessary to collect diffraction patterns with $\mathbf{K}_t$ tilted successively into every second-order Bragg condition in one quadrant of the zone-axis pattern. The remainder can be generated by symmetry operations (which must include both the scattering vector and the crystal). Inversion symmetry is not assumed, since the random start assigns an arbitrary origin.

More generally, a systematic approach to symmetry reduction would be based on finding the irreducible representation of the subgroup of the crystal space group which contains the symmetries of the scattering vector. This allows a matrix **T** to be found as described elsewhere [22] which, through a similarity transform, transforms **A** to block-diagonal form, reducing the dimension of the problem, the number of eigenvectors and eigenvalues, and the number of diffraction patterns needed. Powers of A are also diagonalized by **T**, so this matrix also block-diagonalizes **S**. Crystal space groups may be determined by the methods of convergent-beam diffraction [5].

Our analysis depends crucially on the validity of equations 4 and 5 for the periodicity of Bloch waves in **K**-space. However, these results depend on infinite summations, and become an approximation if the sum is truncated, as for a limited number of beams. The resulting error can be estimated by comparing a simulations for the symmetrical orientation ($\mathbf{K}_t$=0) with those for a different Bragg condition and value of $\mathbf{K}_t$, using different excitation errors on the diagonal, as given in section 2. The central column in a tilted computation with excitation errors corresponding to a particular value of $\mathbf{K}_t$ is compared with the unobserved intensities in the column labelled $\mathbf{K}_t$ for the symmetrical orientation. These predicted Bragg beam intensities agree well with a large number of beams. However, our simulations show that significant errors up to 20% occur on some beams if $N < 10$.

**5. Future developments.**

Experience with phasing X-ray and electron data [17] shows the power of using higher dimensions when using phasing methods based on atomicity, such as flipping, where the density is driven to zero in the space between atoms, and higher dimensionality increases that space (volume). The flipping method thus works far better in 3D rather than 2D. Since curvature of the Ewald sphere provides higher-order reflections, which provide three-dimensional information about the potential, we can expect their inclusion in this algorithm to improve phasing. The inclusion of these reflections in the algorithm is straightforward, using the re-normalization approach described elsewhere [5].

If HOLZ reflections are not included, the large tilts needed to fill **S** will eventually be limited by the incursion into the diffraction pattern of these HOLZ lines and Bragg spots. A simple construction [8] shows that the resolution limit, for a crystal with period c along the beam direction, is $d = \sqrt{\lambda c}$, or a 2 angstrom resolution limit for a protein crystal with period c = 160 angstroms at 200 kV.

The inclusion of a full 2D absorption potential has yet to be considered - here we include only the mean absorption on the diagonal. For a non-centrosymmetric crystal this might contribute additional small real and imaginary parts to every complex structure factor, which must be retrieved. This may be possible, since we note that in [23], logarithmic inversion from such a scattering matrix **A** with absorption is demonstrated.

The ability to distinguish enantiomorphs, or the "hand" of a chiral crystal by TED by taking advantage of multiple scattering was first demonstrated for inorganic crystals (such as quartz) long ago, using the CBED method [6]. Hand refers to the sense of rotation of a helix. Single scattering conditions do not allow this distinction, however the dynamical diffraction patterns are sensitive to hand. Since right-handed alpha-helices are a basic structural unit of all proteins, protein crystals cannot have inversion symmetry (unless combined with artificially produced mirror-related left-handed types within the same crystal). In the drug industry, a failure to create

small molecules with the correct hand can have disastrous consequences for patients, and the ability to distinguish enantiomers in pharmaceutical nanocrystals by TED using multiple scattering has recently been demonstrated [24].

The ability to reconstruct the correct enantiomorph from the magnitudes of the scattering matrix depends highly on the thickness of the crystal. At small thickness, the data is dominated by single scattering, which is not sensitive to chirality. In this case, either "support" (left or right handed) of vacuum space around atoms is equally likely to be reconstructed, and will be consistent with Bragg intensities. At the other extreme, the inversion algorithm is also not sensitive to chirality at very large thickness, where the eigenvalues $\lambda$ of $\mathbf{S}$ are computed from its eigenvectors and magnitudes to avoid the previously mentioned instability when computing $\lambda$ from $\gamma$. In this case, the N-phaser algorithm (along with any inversion algorithm seeking to avoid the eigenvalue instability) essentially seeks a pair ($\mathbf{A}$, $\mathbf{S}$) where $\mathbf{S}$ has the correct magnitudes, $\mathbf{A}$ satisfies the structure matrix symmetry constraints and has the correct diagonal entries, and $\mathbf{A}$ and $\mathbf{S}$ share the same eigenvectors (but not necessarily the same eigenvalues).

To understand this chiral ambiguity in the inversion, define $\mathbf{A}$ and $\mathbf{A}_m$ to be the structure matrices of the correct and mirror enantiomorphs, with eigenvalue decompositions $\mathbf{A} = \mathbf{C\Gamma C}^*$ and $\mathbf{A}_m = \mathbf{C}_m\mathbf{\Gamma}_m\mathbf{C}_m^*$. Due to the time-reversal property of the Fourier transform and Hermitian symmetry of $\mathbf{A}$, we have that $\mathbf{A}_m = \mathbf{A}^T = \overline{\mathbf{A}}$, where $\overline{\mathbf{A}}$ is the entry-wise conjugation of $\mathbf{A}$. Hence, $\mathbf{C}_m = \overline{\mathbf{C}}$ but $\mathbf{\Gamma}_m = \mathbf{\Gamma}$ since the eigenvalues are real. Consequently, the corresponding scattering matrices can be expressed as $\mathbf{S} = \exp(2\pi i\, \mathbf{A}\, t) = \mathbf{C} \exp(2\pi i\, \mathbf{\Gamma}\, t)\, \mathbf{C}^*$ and $\mathbf{S}_m = \exp(2\pi i\, \mathbf{A}_m\, t) = \overline{\mathbf{C}} \exp(2\pi i\, \mathbf{\Gamma}\, t)\, \overline{\mathbf{C}}^*$. Note that both $\mathbf{S}$ and its conjugate $\overline{\mathbf{S}} = \overline{\mathbf{C}} \exp(-2\pi i\, \mathbf{\Gamma}\, t)\, \overline{\mathbf{C}}^*$ have the same magnitudes, and that $\overline{\mathbf{S}}$ has the same eigenvectors as $\mathbf{A}_m$. Consequently, the large thickness algorithm will accept the pair ($\mathbf{A}_m$, $\overline{\mathbf{S}}$) as a valid solution. However, at intermediate thickness, with a moderate amount of coherent multiple scattering, the eigenvectors $\lambda$ can instead be stably computed from $\gamma$ via the complex exponential and the inversion is able to reveal the correct hand of the crystal. In this case, due to the absence of the eigenvalue instability, one can instead enforce that $\mathbf{A}$ and $\mathbf{S}$ have both the same eigenvectors and eigenvalues. Then the pair ($\mathbf{A}_m$, $\overline{\mathbf{S}}$) will not be accepted as a valid solution, as $\mathbf{A}_m$ and $\overline{\mathbf{S}}$ have different eigenvalues.

The extension of this method to non-periodic samples, important for single-particle cryo-EM and the study of defects in inorganic crystals, is under consideration.

**Acknowledgements.**

Thanks to all my co-authors, postdocs and students on all my papers on this subject over the past forty years. Supported by ARO award W911NF2010321, the Advanced Scientific Computing Research and Basic Energy Sciences programs of the Office of Science of Department of Energy (DOE) (Award No. DE-AC02-05CH11231), and by LaboratoryDirected Research and Development funds from Berkeley Lab from the Director, Office of Science DOE (Award No. DE-AC02-05CH11231).

**References.**


1. B. Nanenga and T. Gonen. The cryo-EM method for microcrystal electron diffraction. Nature methods. 16, 369 (2019)

2. J. Hadermann and L. Palatinus Eds. Special issue on Electron Crystallography. Acta Cryst. B75, 462. (2019).

3. H.R. Kolar, J.C.H.Spence and H. Alexander. Observation of moving dislocation kinks and unpinning. Phys. Rev. Letts. 77, 4031. (1966).

4. F. Ross , J.M. Gibson and R. D. Twesten. Dynamic observations of interface motion during oxidation of silicon. Surface Science 310, 243 (1994).

5. J.M. Zuo and J.C.H. Spence Advanced Transmission Electron Microscopy. Springer. New York (2017)

6. Johnson, A.W.S. and Preston, A.R., 1994. Some notes on the selection of structural chirality by CBED. *Ultramicroscopy*, *55*(3), 348. (1994).

7. P. Brazda, L. Palatinus, M. Babor. Electron diffraction determines molecular absolute configuration in a pharmaceutical nanocrystal. Science, 364, 667 (2019).

8. J.J. Donatelli and John C.H. Spence. Inversion of many-beam Bragg intensities for phasing. Phys Rev. Letts. 125, 065502 (2020).

9. J.C.H. Spence, B. Calef and J.M. Zuo Acta Cryst. A55,112 (1999)

10. R. P. Millane and V. L. Lo. Iterative projection algorithms in protein crystallography. Acta Cryst. A69, 517 (2013)

11. H.G. Brown, Z. Chen, M. Weyland, C. Ophus, J. Ciston, L.J. Allen and S.D. Findlay. Phys Rev. Letts. 121, 266102 (2018).

12. L. Sturkey Proc Phys. Soc. 80, 321 (1962)

13. F. Fujimoto, J. Phys Soc Jap. 14, No. 11, p.1558 (1959)

16. C.J. Humphreys, Rep Prog Phys. 42, 1825 (1979).

14. L.J. Allen, T.W. Josefsson and H. Leeb. Acta Cryst. A54, 388 (1998)

15. J.C.H. Spence Acta Cryst. A54, 7 (1998).

16. G. Oszlanyi and A. Suto Acta Cryst. A60, 134 (2004).

17. J.T. McKeown and J.C.H. Spence J. Appl. Phys. 106, 074309 (2009).

18. P. Hirsch, Howie, A. Nicholson, R., Pashley D. and Whelan, M.J. "Electron microscopy of thin crystals". Butterworths. London. (1965). Chapter 10.

19. L.J. Allen, Koch, C., Oxley, M.P. and Spence, J.C.H., 2001. Inversion of dynamical electron scattering to obtain the crystal potential using data from two thicknesses. Acta Crystallographica Section A: Foundations of Crystallography, *57*(4), 473. (2001)

20. A.J.F. Metherell. Electron Microscopy in Materials Science, Volume 1**.** p. 401. Ed. U.Valdre. Ettore Majorana. Commission of European Communities, Brussels. (1975)

21. P.H. Dederichs, Dynamical diffraction theory by optical potential methods. Solid State Physics, Vol. 27 ,135 (Eds H. Ehrenreich, F. Seitz and D. Turnbull). Academic Press, New York.

22. M. Kogiso and H. Takahashi. Group-theoretical methods in many-beam theory of electron diffraction. J. Phys Soc Jap 42, 223 (1977).

23. L.J. Allen, H.M.J. Faulkner and H. Leeb. Acta Cryst. A56, 119 (2000)

24. P. Brazda, L. Palatinus, M. Babor. Electron diffraction determines the molecular absolute configuration in a pharmaceutical nanocrystal. Science, **364** , 667 (2019).